Journal of Mathematical Chemistry, Vol. 42, No. 2, August 2007 (© 2006)
DOI: 10.1007/s10910-006-9085-x

Diffusion without constraints

S. Sauerbrei and P.J. Plath

Institut für Angewandte und Physikalische Chemie – AG Chemische Synergetik, Universität Bremen, Bibliothekstraße NW2, D-28359 Bremen, Germany
E-mail: plath@zfn.uni-bremen.de

Received 14 December 2005; revised 8 February 2006

The consideration of developing open systems, which show structure formation like the temporal development of bubble size distribution during foam decay leads us to a new approach to diffusion processes. In this context, we refer to our articles *The Apollonian Decay of Beer Foam – Bubble Size Distribution and the Lattices of Young Diagrams and their Correlated Mixing Functions* (S. Sauerbrei E.C. Haß, P.J. Plath, Discrete Dynamics in Nature and Society submitted and accepted) and *On the Characterization of Foam Decay with Diagram Lattices and Majorization* (S. Sauerbrei U. Sydow, P.J. Plath Zeitschrift für Naturforschung A, Submitted). By the join of partition diagrams and their permutations a structure is derived, which realizes all possible distributions. Transitions containing negative probabilities become possible and the intrasystem Shannon entropy shows an oscillating behaviour. Our partition-permutation-structure enables a description of positive and negative diffusion processes – or of diffusion processes without constraints. The characteristics of the partition-permutation-structure are comparable to the properties of our foam decay.

KEY WORDS: diagram lattices, foam decay, majorization

AMS subject classification: 03G10

1. Experimental

For our new measurements we take a CCD-camera (CV-M10 CCD camera; lens 0.5×; display detail 1.3×1.0 cm) and a cold light source (KL 2500 LCD). A 20 ml non-foamed beer (*Warsteiner*) at 24±1°C poured in a rectangular glass vessel (2.5×2.5 cm) is frothed up with ultrasound (Ultrasonik 28×; NEY) for 13 s until there is no more increasing foam volume [1]. After frothing up we take pictures of the decaying foam in 10 s intervals. To obtain bubble size distributions from the foam pictures for a statistical evaluation we have acquired as follows: the bubble sizes (bubble diameter $d[10^{-4}\,\mathrm{m}]$) are divided into 10 size intervals, which are normed to unity: ($0 < d < 1.73$: 0.1; $1.73 < d < 3.46$:0.2; $3.46 < d < 5.19$:0.3; ... $13.84 < d < 15.57$:0.9; $15.57 < d$: 1). The ratio of the number of

*Corresponding author.

0259-9791/07/0800-0153/0 © 2006 Springer Science+Business Media, Inc.

bubbles within an interval to the total number of bubbles at time t(s) represents the relative frequency v_i. The consideration of the temporal development of the bubble size distributions and of the Shannon entropy [2], respectively, confirms our last measurements [1]. The treatment with ultrasound leads to a very narrow distribution in the beginning which develops to a multi-model distribution at the end of the rearrangement phase (figures 1–4). In figure 5 the temporal development of the bubble size distributions is plotted as a three-dimensional diagram, which shows very well the oscillating behaviour of single bubble size intervals.

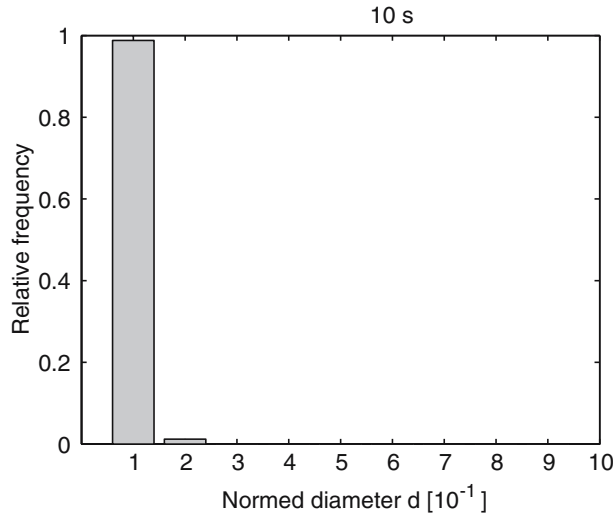

Figure 1. The narrow bubble size distribution 10 s after being frothed up with ultrasound.

Figure 2. The corresponding foam picture of the narrow bubble size distribution after 10 s.

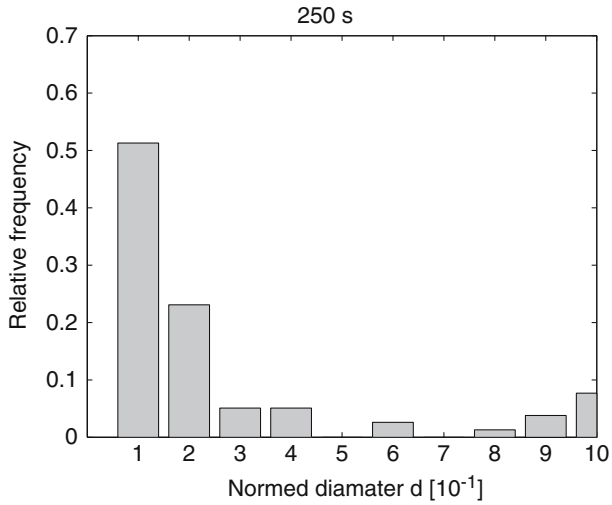

Figure 3. The multi-modal bubble size distribution after 250 s.

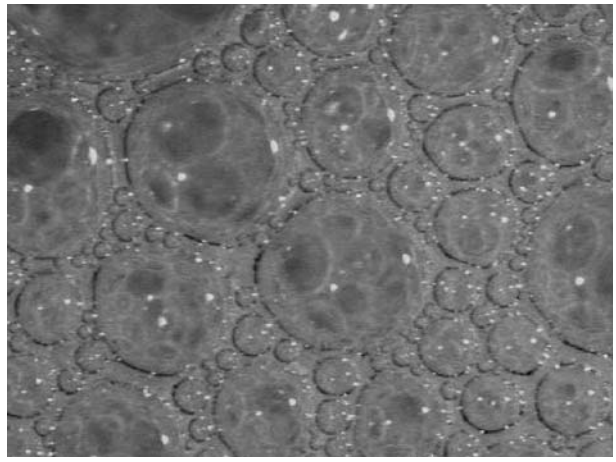

Figure 4. The foam picture of the multi-modal bubble size distribution after 250 s.

The Shannon entropy I (equation (1)) of the bubble size distributions increases up to a maximum and oscillates more or less (see figure 6).

$$I(\gamma) = -\sum_{i=1}^{n} v_i l d v_i . \tag{1}$$

The multi-model distribution at the end of the rearrangement phase of the foam and the oscillating behaviour of the Shannon entropy are significant characteristics of the temporal development of the bubble size distributions and these characteristics are representative for a lot of different beers.

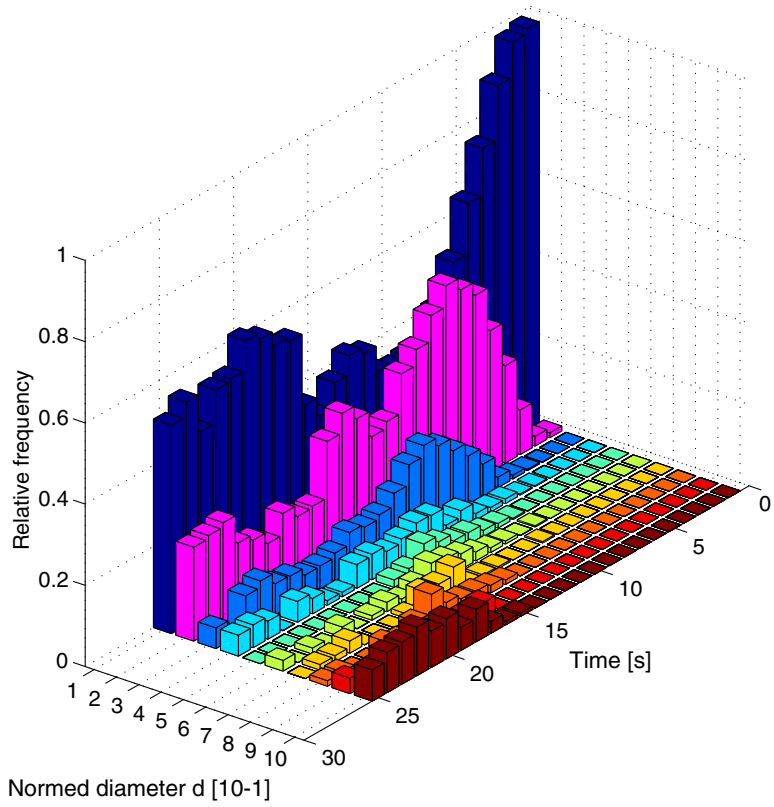

Figure 5. The temporal development of the bubble size distributions as a three-dimensional diagram.

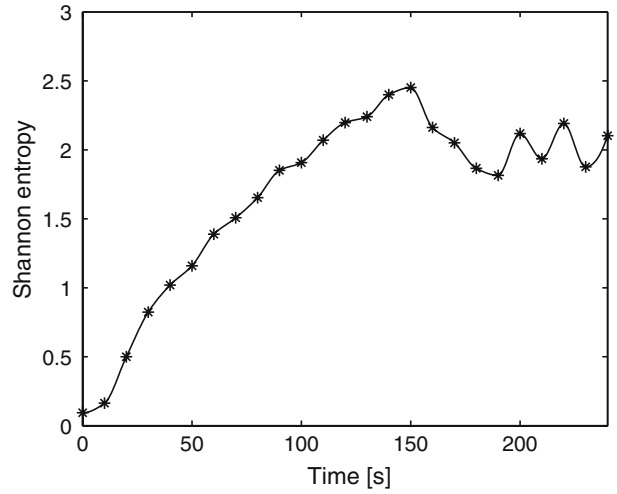

Figure 6. The temporal Shannon entropy development of the bubble size distributions shown in figure 5 exhibits a more or less oscillating behaviour.

Another characteristic is the complicated exponential decay of the foam volume [1], which is measured for *Warsteiner Beer* too. In table 1, we see the coefficients b and c of the exponential decay law of higher order (equation (2))

$$V = V_{0,0} \exp(-bt - ct^{2.5}) \tag{2}$$

Table 1
The coefficients of the exponential decay law of higher order $V = V_{0,0} \exp(-bt - ct^{2.5})$ in equation (2) and of the single processes: *drainage* $V_1 = V_{0,1} \exp(-bt)$ in equation (3) and *rearrangement* $V_2 = V_{0,2} \exp(-ct^{2.5})$ in equation (4) for *Warsteiner Beer*. The decay is measured at different temperatures T (22±1°C, 10±1°C and 0±1°C) and for different sizes of measuring cylinders (100 ml with diameter $d = 2.6$ cm, 250 ml with $d = 3.6$ cm, and 500 ml with $d = 5.0$ cm) combined with certain initial volumes V_0 of non-foamed beer: 20 ml non-foamed beer in the 100 ml measuring cylinder (20/100), 50 ml in the 250 ml measuring cylinder (50/250), and 100 ml in the 500 ml measuring cylinder (100/500) are frothed up with ultrasound. We like to express the notation 20/100, 50/250 and 100/500 with $k = V_0/d$: $k(20/100) = 0.7[10^{-3}\,\mathrm{m}^2]$, $k(50/250) = 1.4[10^{-3}\,\mathrm{m}^2]$ and $k(100/500) = 2.0[10^{-3}\,\mathrm{m}^2]$.

T[°C]	$k = V_0/d$ [10^{-3} m^2]	Equation	$V_{0,i}$	b	c
22±1°C	0.7	V	38.73	5.4×10^{-3}	4.7×10^{-7}
		V_1	39.47	6.29×10^{-3}	
		V_2	20.00		1.13×10^{-6}
	1.4	V	93.59	3.57×10^{-3}	2.56×10^{-7}
		V_1	96.08	4.37×10^{-3}	
		V_2	50.00		5.13×10^{-7}
	2.0	V	214.30	3.11×10^{-3}	1.02×10^{-7}
		V_1	219.90	3.66×10^{-3}	
		V_2	110.00		2.61×10^{-7}
10±1°C	0.7	V	43.42	3.11×10^{-3}	4.3410^{-7}
		V_1	44.60	4.11×10^{-3}	
		V_2	28.56		7.50×10^{-7}
	1.4	V	99.00	2.88×10^{-3}	2.87×10^{-7}
		V_1	101.60	3.69×10^{-3}	
		V_2	58.73		4.86×10^{-7}
	2.0	V	208.90	2.60×10^{-3}	2.13×10^{-7}
		V_1	214.60	3.35×10^{-3}	
		V_2	129.80		3.85×10^{-7}
0±1°C	0.7	V	35.16	2.98×10^{-3}	3.99×10^{-7}
		V_1	36.15	3.97×10^{-3}	
		V_2	22.00		6.36×10^{-7}
	1.4	V	80.23	2.52×10^{-3}	2.53×10^{-7}
		V_1	82.36	3.30×10^{-3}	
		V_2	52.92		4.42×10^{-7}
	2.0	V	167.00	2.94×10^{-3}	1.39×10^{-7}
		V_1	171.00	3.52×10^{-3}	
		V_2	95.12		3.14×10^{-7}

for different temperatures T (22±1°C, 10±1°C and 0±1°C) and different sizes of measuring cylinders (100 ml with diameter $d = 2.6$ cm, 250 ml with $d = 3.6$ cm, and 500 ml with $d = 5.0$ cm) combined with certain initial volumes V_0 of non-foamed beer (20 ml non-foamed beer in the 100 ml measuring cylinder denoted by 20/100, 50 ml in the 250 ml measuring cylinder, 50/250 and 100 ml in the 500 ml measering cylinders, 100/500), which are frothed up with ultrasound. Here, we like to introduce a new notation: let k be the ratio V_0/d of the initial volume of the non-foamed beer V_0 and the measering cylinder diameter d. Then we obtain $k(20/100) \approx 0.7[10^{-3}\text{m}^2]$, $k(50/250) \approx 1.4[10^{-3}\,\text{m}^2]$ and $k(100/500) = 2.0[10^{-3}\,\text{m}^2]$. Additionally, the coefficients b and c of the single processes drainage and rearrangement in equations (3) and (4) are shown in table 1.

$$\text{Drainage}: \qquad V_1 = V_{0,1}\exp(-bt) \tag{3}$$

and

$$\text{Rearrangement}: \qquad V_2 = V_{0,2}\exp(-ct^{2.5}), \tag{4}$$

where $V_{0,2}$ in equation V_2 (equation. (4)) is fictitious in contrast with $V_{0,0}$ (equation (2)) and $V_{0,1}$ (equation (3)), which are approximately of the same size and describe the foam volume after frothig up with ultrasound. The $V_{0,2}$ characterizes the fictitious volume in the beginning of the rearrangement phase of the foam decay by non-considering the drainage process. It is easy to see that V in equation (2) is a function of V_1 and V_2 in equations (3) and (4) [1]:

$$V = f(V_1, V_2). \tag{5}$$

We like to conclude the results of our table 1: considering the coefficient b of the functions V (equation (2)) and V_1 (equation (3)) we see that with increasing $k^{\uparrow}$ and constant temperature T_{const} this coefficient diminishes, $b^{\downarrow}$. This does not hold for 0 ± 1°C. At 0±1°C there is no general tendency for the coefficient b. The coefficient c of the functions V (equation (2)) and V_2 (equation (4)) has the same trend. If $k^{\uparrow}$ increases, the coefficient $c^{\downarrow}$ decreases and this trend holds for all temperatures T. If we let k_{const} constant and change the temperature T, one can take from table 1 that with decreasing temperature $T^{\downarrow}$ the coefficient $b^{\downarrow}$ decreases too, except the outlier 100/500 at 0±14°C. Under these equal terms the coefficient c behaves with no tendency. Comparing both coefficients with constant k_{const} and T_{const} one can see that the b of V is always smaller than the b of V_1 and the c of V is less than c of V_2. This is characteristic of the functions V and V_1, respectively, V and V_2. It follows a summary and an interpretation of the results:

T_{const}	$k^{\uparrow}$	$b^{\downarrow}$	The smaller b the slower the drainage with increasing initial beer volume V_0 relative to the vessel diameter.

			This does not hold for $T = 0 \pm 1°C$.
T_{const}	$k^{\uparrow}$	$c^{\uparrow}$	The smaller c the slower the rearrangement with increasing initial beer volume V_0 relative to the vessel diameter.
k_{const}	$T^{\downarrow}$	$b^{\downarrow}$	With lowering the temperature of the beer the drainage becomes slower.
k_{const}	$T^{\downarrow}$	c	There is no influence of the temperature on the coefficient c.

One can find a detailed description of these processes and their coefficients for *Beck's beer* in our paper *The Apollonian Decay of Beer Foam – Bubble Size Distribution and the Lattices of Young Diagrams and their Correlated Mixing Functions* [1].

2. Partition diagrams and their permutations

Our paper *On the Characterization of Foam Decay with Diagram Lattices and Majorization* [3] has shown that partition diagrams can be mapped on probability distributions and the temporal development of our bubble size distributions is comparable to the progression in a partition diagram lattice generated by Ruch [4]; we called these lattices *Ruch lattices*. The partition diagrams were represented as partition vectors extented with zero elements so that all partition vectors of the number n have the dimension n. These vectors $\gamma = (\gamma_i)$ rearranged in decreasing order of their components have the same trace that means the sum of the vector components is n: $\sum_{i=1}^{n} \gamma_i = n$ (equation (7)). To compare these vectors γ one can sum them partially as in equation (6).

$$\sum_{i=1}^{k} \gamma_i^{\star} \geqslant \sum_{i=1}^{k} \gamma_i'^{\star}; \qquad k = 1, 2, \ldots, n-1 \tag{6}$$

and

$$\sum_{i=1}^{n} \gamma_i = \sum_{i=1}^{n} \gamma_i', \tag{7}$$

where $\gamma^{\star} = (\gamma_1^{\star}, \gamma_2^{\star}, \ldots, \gamma_n^{\star})$ denotes the n-tuple rearranged in non-increasing order, $\gamma_1^{\star} \geqslant \gamma_2^{\star}, \geqslant \cdots \geqslant \gamma_n^{\star}$ (we can say that $\gamma^{\star}$ denotes the partition vectors of a Ruch lattice and γ denotes all partition vectors that means γ includes $\gamma^{\star}$ and its permutations). The comparisons of the vectors $\gamma^{\star}$ in equations (6) and (7) are denoted by $\gamma' \prec \gamma$, which means that γ majorizes γ'. These equations are the basic conditions of the classical majorization of Muirhead [5], Hardy et al. [6]. The classical majorization was discussed in detail in our paper [3] and will be expanded in section 3. By the componentwise comparison of the partial sum vectors Ruch defined lattice structures of partition diagrams, which are

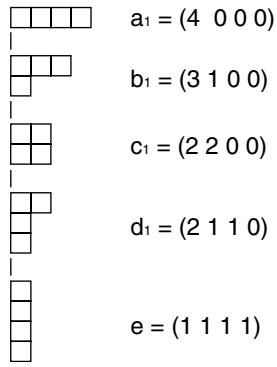

Figure 7. Totally ordered partition diagram lattice for $n = 4$ and corresponding partition vectors.

totally ordered, and partially ordered, respectively. Partially ordered lattices he obtained for $n \geqslant 6$, which show so-called incomparable diagrams not holding equation (6). He mentioned the permutations of partition diagrams that means the sequence of the partition vector entries changes, but he did not take into account these permutation diagrams for the lattice structures. He considered a partition diagram as a representative of its permutations. We like to include these permuted partition diagrams and vectors $\gamma = (\gamma_i)$, respectively, to this lattice structures of Ruch and have to change the condition in equation (6) so that the partition vectors with their permutations $\gamma(\gamma^\star \subset \gamma)$ are not sorted as $\gamma^\star$. It is clear that the traces do not change. Then we obtain equations (8) and (9):

$$\sum_{i=1}^{k} \gamma_i \geqslant \sum_{i=1}^{k} \gamma_i'; \quad k = 1, 2, \ldots, n-1 \tag{8}$$

and

$$\sum_{i=1}^{n} \gamma_i = \sum_{i=1}^{n} \gamma_i'. \tag{9}$$

Otherwise it is the same procedure: a partition diagram as a partition vector is expanded with zero elements and can be permuted. Then we define an order and partial order, respectively, by computing and comparing the partial sum vectors of the partition vectors.

It is important to distinguish between the set of the partition diagrams, the set of the permutations of one partition diagram, and the set of the partition diagrams and their permutations. The set of the partition diagrams of $n = 4$ with corresponding partition vectors are shown in figure 7 and characterize a totally ordered lattice. These structures were shown in the works by Ruch [4, 7, 8] and in our article [3].

In figures 8 and 9, we see the permutation frameworks of the partition vectors for $n = 4$. With reference to the frameworks in figures 8 and 9, one has to differ between the permutations without changing the order of the non-zero elements of one partition vector (the subsets of the permutations) and all permutations of one partition vector. Figure 8 shows the permutation subsets of the

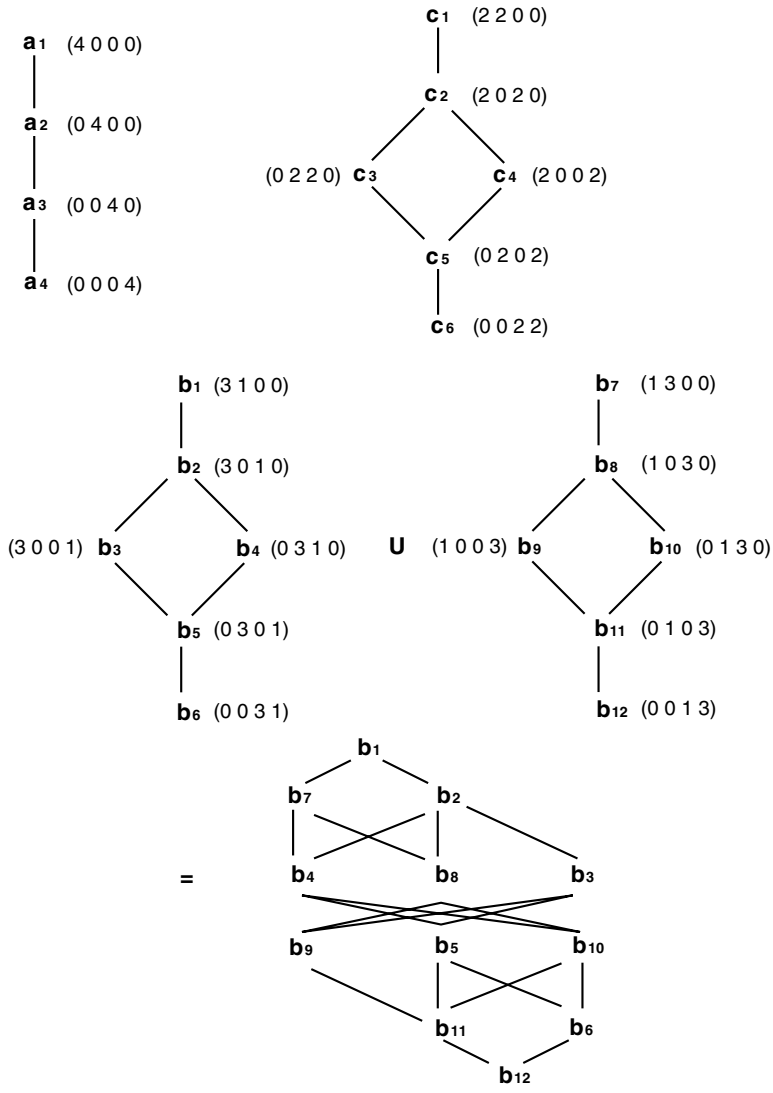

Figure 8. The permutation structures and their subsets of the partition vectors a_i = (4 0 0 0), b_i = (3 1 0 0) and c_i = (2 2 0 0). The number of the permutations of one partition vector can be computed by the formula $P_{n,n_1,n_2,\ldots} = \frac{n!}{n_1!n_2!n_3!\ldots}$, whereas the number of factors n_i in the denominator is given by the number of sets of equal elements.

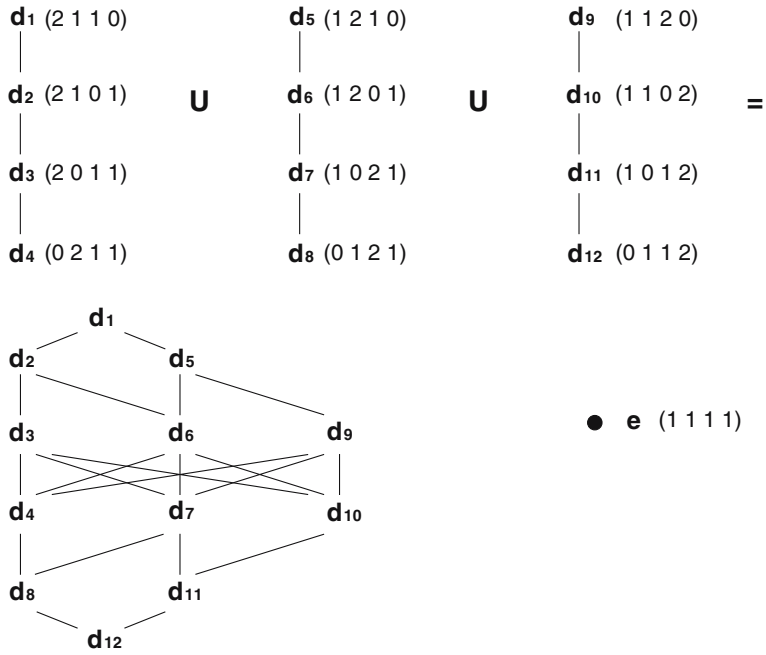

Figure 9. The permutation structure and its subsets of the partition vector $d_i = (2\ 1\ 1\ 0)$ and the vertex $e = (1\ 1\ 1\ 1)$.

partition vectors b_1–b_6 and b_7– b_{12} and their join during the propositional calculus is changing. In figure 9, we see the subsets of the d_i-vectors. Although the number of permutations of d_i is the same as of b_i, the structures differ and the subsets too. It is very interesting that permutations of partition vectors can be assigned to totally and partially ordered structures. The notation of a_1 to a_4, b_1 to b_{12}, c_1 to c_6, d_1 to d_{12} and e is given as partition diagrams in figure 10, which shows the three-dimensional framework of the set of the partition diagrams and their permutations as a two dimensional projection in the plane. The same structure we see in figure 11 as a three-dimensional structure projected stereographically for better understanding. The latter two structures are the join of the structures in figures 8 and 9. Here the generating principle of the structures above summarized: each set of vectors can be compared by the partial sums (equation (6) with reference to the sorted partition vectors $\gamma^\star$ of a Ruch lattice and equation (8) with reference to the permuted partition vectors γ without any order of the components; $\gamma^\star \subset \gamma$. The lattice structures describe what diagrams are contained in other diagrams. The join of two sets means that all vectors of these sets are taken into account during the partial sum comparison).

As aforementioned the structure of the partition diagrams and their permutations – we will call it (***p****artition-****p****ermutation-structure*) pp-structure – can be

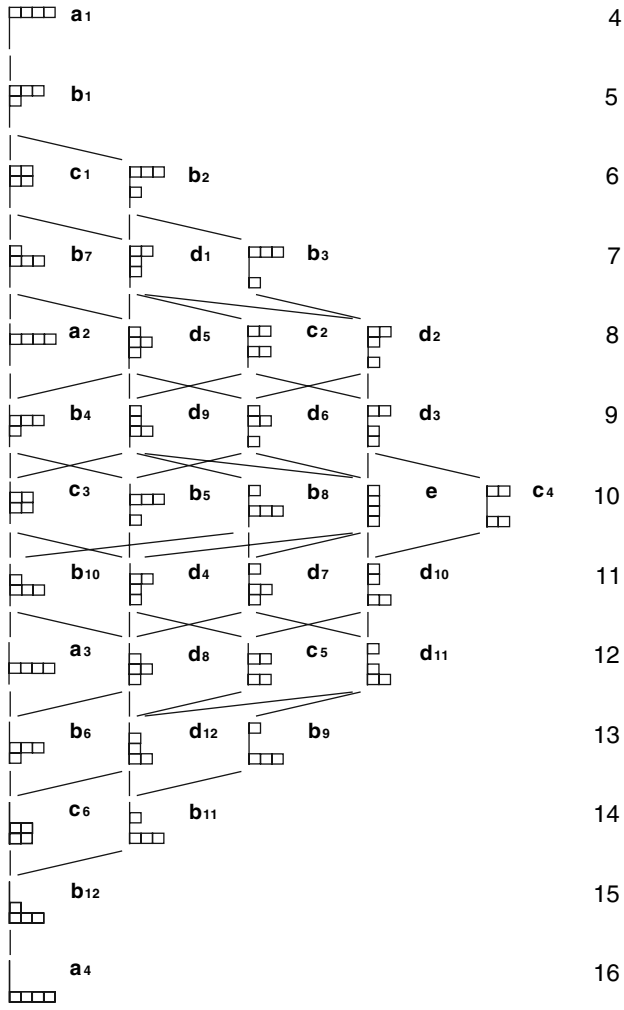

Figure 10. The structure of the set of the partition diagrams and their permutations as a two-dimensional projection. Later we will see that the diagrams represent macrostates of four tetrahedron dices with the numbers 1–4 (figure 16). The numbers on the right side are the sums of the macrostate numbers, (table 4).

computed by comparing the partial sum vectors of these diagrams. But it is easy to see that this pp-structure can also be constructed by the following algorithm:

> *A diagram γ is called greater than a diagram γ', if γ can be constructed from γ' by moving boxes exclusively upward, i.e. from row n to row $(n-i)$ with $n > i$ or in other words, from any row n containing at least one box, one box moves upward to the higher row $(n-1)$, if one begins at the greatest lower bound.*

We see an example for the algorithm of the pp-structure in figure 12. Feel free to compute the pp-structure for $n = 5$.

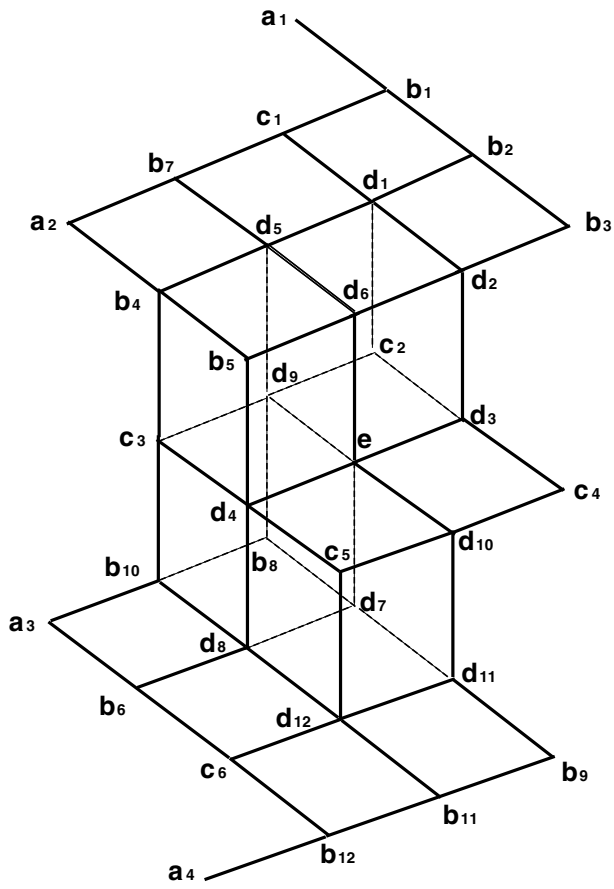

Figure 11. The set of the partition diagrams and their permutations as a three-dimensional lattice structure projected stereographically.

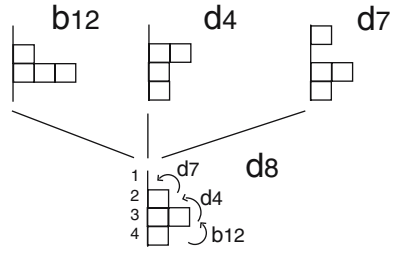

Figure 12. An example for the algorithm using the diagram d_8, which transforms into the diagrams b_{12}, d_4 and d_7 by moving one box from row n to row $(n-1)$.

3. The characteristics of the PP-structure

The pp-structure in figure 10 shows exceptional characteristics. We like to point out the differences between this structure and the set of the partition diagrams (figure 7): we map diagrams onto distribution functions and the diagram progression to a diffusion process.

3.1. Join, meet and shannon entropy

The least upper bound (join or $lub = a_1$) and the greatest lower bound (meet or $glb = e$) of the partition diagrams characterize a distribution with maximum order, i.e. all elements are in the same state (*lub*) or all boxes are in one row and an equal distribution (*glb*), i.e. in each row is one box. One can think about this progression from *lub* to *glb* of the partition diagram lattice in figure 7 as an ordinary diffusion process. However, both the *lub* (a_1) and the *glb* (a_4) of the pp-structure in figure 10 characterize a distribution with maximum order, but they differ in the state (i.e. row number n). Here the equal distribution e is centered in the pp-structure.

If we consider the Shannon entropy I (see equation (1) [2, 4]) of the partition diagram progression from *lub* to *glb* (figure 7), we see that I is monotonically increasing (table 2).

On the other hand, the non-monotonical Shannon entropy development of the pp-structure (figure 10) behaves more or less oscillating. We know $I(a_1, \ldots, a_4) < I(b_1, \ldots, b_{12}) < I(c_1, \ldots, c_6) < I(d_1, \ldots, d_{12}) < I(e)$ and consider for instance the left column of the two-dimensional representation of the pp-structure (figure 10) and its Shannon entropy development (figure 13). This is only one possible path, if one begins at partition diagram a_1 (*lub*) and ends at partition diagram a_4 (*glb*). But one does not have to end at diagram a_4, one can end at diagram e too. The partition diagram e is the so-called point of no return [3] because there exists no $(n \times n)$-stochastic matrix (transition), which maps diagram e on another diagram. In the following we like to consider all stochastic matrices and transitions, respectively, with their characteristics.

Table 2
The monotonically increasing Shannon entropy I of the partition diagrams in figure 7.

Partition diagram	a_1	b_1	c_1	d_1	e
Shannon entropy I	0.0000	0.8113	1.0000	1.5000	2.0000

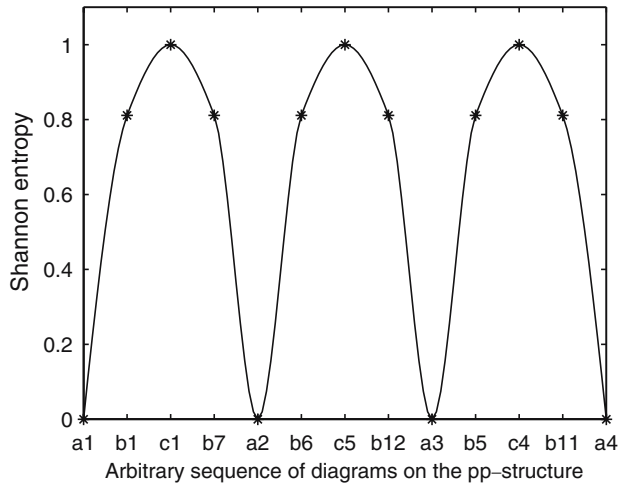

Figure 13. One possible path on the pp-structure from *lub* to *glb* (left column of the two-dimensional projection of the pp-structure). The Shannon entropy of this particular progression is oscillating.

3.2. *Stochastic matrices as transitions between diagrams*

The transitions between all diagrams of the pp-structure in figure 10 are defined by doubly stochastic matrices (dsm), their inverses (dsm^{-1}), pseudo doubly stochastic matrices ($pdsm$), or permutation matrices (pm) with ϵ as the identity matrix. The stochastic matrices can be invertible (reversible ($rev-$) transition) or non-invertible (irreversible ($irr-$) transition). Impossible transitions are denoted by $\times$. These transitions are impossible because there exists no $n \times n$ matrix M with only positive (dsm, pm) or positive and negative (mixed) entries (dsm^{-1}, $pdsm$) and additionally the matrix holds that its row and column sums are one. A transition becomes impossible if one starts from diagram e. One ought to change the matrix and vector dimension to obtain a transition, which is described by a $pdsm$. An example for an impossible transition, which becomes possible by expanding the dimension is given in equation (10).

$$M_{2,2}\begin{pmatrix}1\\1\end{pmatrix} \neq \begin{pmatrix}2\\0\end{pmatrix}; \qquad M_{3,3}\begin{pmatrix}1\\1\\0\end{pmatrix} = \begin{pmatrix}2\\0\\0\end{pmatrix}; \qquad M_{3,3} = \begin{pmatrix}2 & 0 & -1\\ -1 & 1 & 1\\ 0 & 0 & 1\end{pmatrix}. \quad (10)$$

But now we will not go into the particulars of this transitions starting from diagram e. Table 3 represents all transitions of the pp-structure reading from left to right that means in rows. We note [3] that transitions (dsm, dsm^{-1}, $pdsm$, pm) in each direction between partition diagrams of a *Ruch lattice* (figure 7) [4] are possible, if one does not arrive at the point of no return e. Hence, the transitions between each diagram in each direction are defined and have to permuted

Table 3
The transitions between all diagrams in each direction of the pp-structure in figure 10 reading from left to right (in rows).

	a_i	b_i	c_i	d_i	e
a_i	pm	$rev-dsm$	$irr-dsm$	$rev-dsm$	$irr-dsm$
b_i	$rev-dsm^{-1}$	pm	$irr-dsm$	$rev-dsm$	$irr-dsm$
c_i	$rev-pdsm$	$irr-pdsm$	pm	$irr-dsm$	$irr-dsm$
d_i	$rev-dsm^{-1}$	$rev-dsm^{-1}$	$irr-pdsm$	pm	$irr-dsm$
e	$\times$	$\times$	$\times$	$\times$	ϵ

with a permutation matrix to obtain the transitions for the pp-structure (figure 10) in table 3.

The doubly stochastic matrices can be generated by the theorems of Muirhead [5] and of Hardy et al.[6], which we have discussed in [3] in detail. The *pdsm* are products of *dsm* and inverse *dsm* and can contain positive and negative entries, in which the column and row sums of a *pdsm* are one. These *pdsm* are essential for irreversible transitions defined by non-invertible *dsm*, which we like to make reversible. By making certain transitions reversible transitions between incomparable partition diagrams become possible. In figure 14 an example is shown for generating a *pdsm* for two incomparable partition diagrams. Note, that we refer to partition diagram lattices [4] without permutations and that we can permute the resulting matrices (transitions) to obtain the matrices for a pp-structure (figure 10). We see (figure 14) that there is always an invertible *dsm* (reversible transition) between the *lub*-diagram (vector $(n\ 0 \ldots 0)$) and the diagram before the

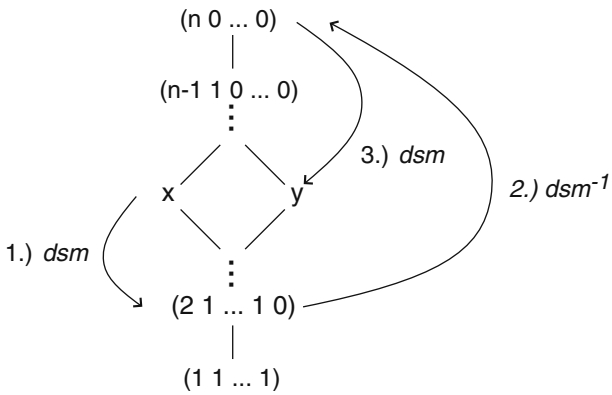

Figure 14. An example for generating a *pds*-matrix (*pdsm*) characterizing the transition between the incomparable diagrams x, y of a partition diagram lattice [4].

point of no return (vector (2 1 . . . 1 0)). Consequently, one can begin for instance at a diagram x belonging to two incomparable diagrams x, y, then go to the diagram before the *glb* (1.) *dsm*). Then the transition to the *lub* follows (2.) dsm^{-1}) and the last transition is the (3.) *dsm*) to diagram y. The product of these transitions (1.), 2.), 3.)) and matrices, respectively, is a *pdsm*. This is only one possible path to obtain the transition matrices, which have as product a *pdsm*. We conclude, that, if transitions between incomparable diagrams are possible, we have to allow *pdsm* with positive and negative components.

3.3. *Positive and negative diffusion*

The stochastic matrices, which we have considered allow transitions between diagrams, but if we take into account that partition diagrams are comparable to probability distributions, then the entries of these matrices characterize transition probabilities. It seems to be unusual defining negative probabilities (dsm^{-1}, *pdsm*), but we will discuss it in the following.

At first, reversible transitions in each direction between almost all diagrams of the pp-structure can only be defined, if we allow stochastic matrices with positive and negative entries. We know that this statement does not hold for the diagram e (equal distribution). Additionally, we like to allow transitions between incomparable diagrams and this is only possible with *pdsm*. But what do these negative entries of the matrices mean? If one considers the diagram progression with its transitions of figure 15, for example – which was already described by the Shannon entropy in figure 13 – it is clear, that in the beginning (a_1 to c_1) the diagrams follow an ordinary (positive) diffusion process as it can be stated for the diagrams in figure 7. The further progression (c_1 to a_2) (figures 10 and 13) is exactly the opposite of a positive diffusion process. The boxes and elements, respectively, develop with increasing order. This behaviour can be seen as oscillations of the Shannon entropy in figure 13. A maximum order of a distribution means a minimal Shannon entropy.

This development of increasing order of the boxes (elements) and decreasing Shannon entropy of the diagrams (distributions) characterizes a negative diffusion process. In figure 15, an example for transitions of negative diffusion is

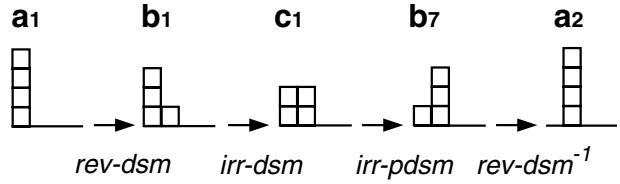

Figure 15. Partition diagrams of the pp-structure characterize positive diffusion and negative diffusion. Additionally we see the transitions (matrices) of these processes.

given; we see the transitions from diagram c_1 to b_7 and from b_7 to a_2, which are matrices with negative and positive components ($irr - pdsm$ and $rev - dsm^{-1}$).

Now we consider the bubble size distributions (histograms) normed to unity with their temporal development: at the beginning after frothing up of the non-foamed beer the Shannon entropy of the histograms increases monotonically to a maximum and after a while shows an oscillating behaviour (figure 6). That is, at the beginning the histograms follow a positive diffusion process (increasing Shannon entropy), but in the rearrangement phase the histograms become incomparable due to the Apollonian structure formation [1] and the Shannon entropy increases and decreases by turns. Otherwise there are histograms h at the time t_i, which form and are majorized by histograms h at the time $t_{i+1} : h(t_i) \prec h(t_{i+1})$, that is, we can consider negative diffusion. It is important to mention, that in case of a transition between two incomparable histograms the Shannon entropy can increase or decrease, i.e. we cannot distinguish between positive diffusion process, respectively, negative diffusion process therein, although the Shannon entropy changes. But one can assume that if the Shannon entropy distinctly increases (decreases) there is a positive diffusion process (negative diffusion process).

We conclude: transitions with negative probabilities (defined by matrices with negatives and positive entries) are peculiar for the pp-structure. This enables a negative diffusion process and transitions between incomparable diagrams and leads to more degrees of freedom for the developing system. The pp-structure characterizes diffusion processes in open systems like foam decay with its corresponding bubble size distributions, which eventually leads to multi-modal distributions and show structure formation. To describe these characteristics it is necessary to include permutations of the corresponding partition diagrams. The same holds for the Shannon entropy with its oscillating behaviour.

4. The PP-structure diagrams as macrostates

The pp-structure is even more than a novel approach to diffusion processes with their distribution functions in open systems. The partition diagrams and their permutations characterize the macrostates of four tetrahedron dices with the numbers 1–4, which are comparable to the row number n, figure 16 and table 4. The macrostates can be computed by the formula of combination with replacement $C_{n,i}$:

$$C_{n,i} = \binom{n+i-1}{i} = \binom{2n-1}{n} = \frac{(2n-1)!}{n!(n-1)!}, \tag{11}$$

where i is the number of items taken from n elements, here is $i = n$ because we take all dices (boxes) into account. (One could take only two dices or boxes $i = 2$ and combine them with the rows. One would obtain 10 combinations.) If

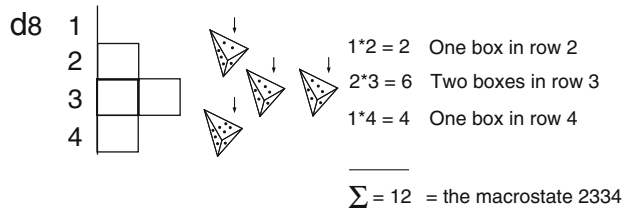

Figure 16. The d_8 diagram is comparable to a macrostate. The boxes correspond to four tetrahedron dices and the row number shows the eye number of the corresponding dice (arrows). The sum of the dice eyes is a characteristic value and decribes the planes of incomparable diagrams in figure 10.

Table 4
The 35 macrostates of four tetrahedron dices. The first column shows the sum of the eye numbers of the dices, the second column shows the macrostates. We see the number of the macrostates of one row in the third column and the number of the microstates (indices) of one row in the fourth column. The configuration of the macrostates is the same as in the pp-structure (figures 10 and 16). The number of the macrostates is given by the formula of combination with replacement $C_{n,i} = (\binom{2n-1}{n})$, with $i = n$, and the number of the microstate can be generated by the formula of variation with replacement $V_{n,i} = n^i = n^n = 4^4 = 256$ with $i = n$.

4	1111_1					1	1
5	1112_4					1	4
6	1122_6	1113_4				2	10
7	1222_4	1123_{12}	1114_4			3	20
8	2222_1	1223_{12}	1133_6	1124_{12}		4	31
9	2223_4	1233_{12}	1224_{12}	1134_{12}		4	40
10	2233_6	2224_4	1333_4	1234_{24}	1144_6	5	44
11	2333_4	2234_{12}	1334_{12}	1244_{12}		4	40
12	3333_1	2334_{12}	2244_6	1344_{12}		4	31
13	3334_4	2344_{12}	1444_4			3	20
14	3344_6	2444_4				2	10
15	3444_4					1	4
16	4444_1					1	1
						$\sum = 35$	$\sum = 256$

we consider the dices as individuals, we obtain the microstates. The microstates can be computed by the formula of variation with replacement $V_{n,i} = n^i = n^n = 4^4 = 256$ with $n = i$.

Now the macrostates can be applied to bubble size distributions. The dices are the bubbles and the eyes of the dices (row number n) are the bubble size intervals. That is clear, if one considers figure 16. Remarkably, the connections between the macrostates which are governed by chance can be described by the partial order (pp-structure).

5. Further possibilities for negative probabilities

There are several reasons to introduce transitions with positive and negative probabilities, that means matrices with negative components like inverse doubly stochastic matrices (dsm^{-1}) and pseudo doubly stochastic matrices ($pdsm$). Firstly, we say a transition is reversible, if its corresponding dsm is invertible and we obtain a dsm^{-1}. If the dsm is not invertible we need a $pdsm$ to define this reversible transition. To make all diagrams of the pp-structure accessible from random initial diagrams, all transitions have to be defined reversible. Such transitions can be experimentally found in the temporal development of our bubble size distributions, except the transitions to the equal distribution and transitions starting from the equal distribution.

Secondly, there are bubble size distributions, which behave as incomparable diagrams. The transitions between incomparable diagrams can only be defined by $pdsm$. Incomparable diagrams occur predominantly at the end of the rearrangement of the foam decay. In this phase of the foam decay the bubble volumes can change by the diffusion of gas across films. The gas flux from high to low-pressure bubbles is set by Laplace's law: $\Delta p = 4\sigma/r$. That means, small bubbles shrink and large bubbles grow, and distributions become incomparable (see, e.g. figure 17 and equation (12).

$$\gamma_\sigma = \begin{pmatrix} 2 \\ 4 \\ 6 \\ 6 \\ 6 \\ 6 \end{pmatrix} \begin{matrix} < \\ = \\ > \\ = \\ = \\ = \end{matrix} \begin{pmatrix} 3 \\ 4 \\ 5 \\ 6 \\ 6 \\ 6 \end{pmatrix} = \gamma'_\sigma. \tag{12}$$

If we take into account that the total number of bubbles decreases during the decay process, one can suppose that the temporal development of the bubble size distributions is a diffusion process with a sink term S.

$$\frac{\partial c}{\partial t} = D\Delta c + S. \tag{13}$$

To define transitions between distributions with decreasing number of elements (bubbles) there is the possibility of the *weak majorization*. We know the meaning of the *classical majorization*:

$$\sum_{i=1}^{k} \gamma_i^\star \geqslant \sum_{i=1}^{k} \gamma_i'^\star; \quad k = 1, 2, \ldots, n-1 \tag{14}$$

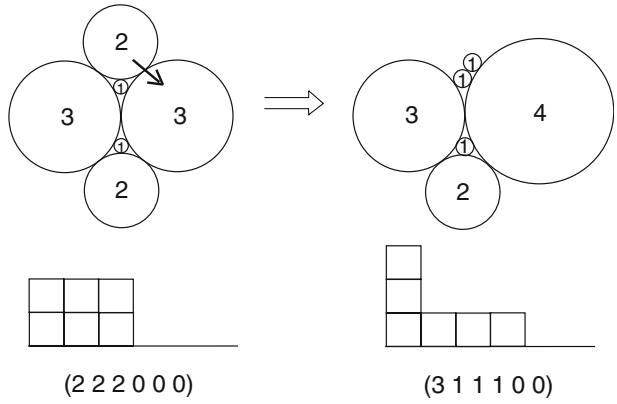

Figure 17. The gas flux goes from high to low-pressure bubbles is set by Laplace's law: $\Delta p = 4\sigma/r$. Large bubbles grow on cost of small bubbles which shrink. We see two bubbles each of the sizes one, two and three and the corresponding diagram with the vector $\gamma = (2\ 2\ 2\ 0\ 0\ 0)$ on the left. On the right the bubble sizes have changed to three bubbles of the size one and one bubble each of the sizes two, three and four because of gas diffusion (arrow) and the diagram with its vector $\gamma' = (3\ 1\ 1\ 1\ 0\ 0)$. In equation (12) the comparison of the partial sum vectors γ_σ and γ'_σ shows the vectors γ and γ' are incomparable.

and

$$\sum_{i=1}^{n} \gamma_i = \sum_{i=1}^{n} \gamma'_i, \tag{15}$$

where $\gamma^\star = (\gamma_1^\star, \gamma_2^\star, \ldots, \gamma_n^\star)$ denotes the n-tuple rearranged in non-increasing order, $\gamma_1^\star \geqslant \gamma_2^\star, \geqslant \cdots \geqslant \gamma_n^\star$.

"The relations (14) and (15) are saying that γ' is majorized by γ, ($\gamma' \prec \gamma$). For a set $\mathbb{A} \subset \mathbb{R}^n$, $\gamma' \prec \gamma$ on $\mathbb{A}$ means $\gamma', \gamma \epsilon \mathbb{A}$ and $\gamma' \prec \gamma$. Replacement of the equality in (15) by corresponding inequality leads to the concept of *weak majorization*. Let $\gamma_{[i]}$ denote the decreasing rearrangement of γ and let $\gamma_{(i)}$ denote the increasing rearrangement of γ.
For $\gamma, \gamma' \epsilon \mathbb{R}^n$,

$$\gamma' \prec_w \gamma \qquad \text{if} \qquad \sum_{1}^{k} \gamma'_{[i]} \leqslant \sum_{1}^{k} \gamma_{[i]}, \qquad k = 1, \ldots, n \tag{16}$$

and

$$\gamma' \prec^w \gamma \qquad \text{if} \qquad \sum_{1}^{k} \gamma'_{(i)} \geqslant \sum_{1}^{k} \gamma_{(i)}, \qquad k = 1, \ldots, n. \tag{17}$$

In either case, γ' is said to be *weakly majorized* by γ (γ *weakly majorizes* γ'). More specifically, γ' is said to be *weakly submajorized* by γ if $\gamma' \prec_w \gamma$ and γ' is said to be *weakly supermajorized* by γ if $\gamma' \prec^w \gamma$.
$\gamma' \prec_w \gamma$ ($\gamma' \prec^w \gamma$) on $\mathbb{A}$ means $\gamma', \gamma \epsilon \mathbb{A}$ and $\gamma' \prec \gamma$. The origins of the terms "submajorized" and "supermajorized" lie in the following limited characterizations of weak majorization in terms of linear transformations:

$$\gamma' \prec_w \gamma \text{ on } \mathbb{R}^n_+ \text{ if and only if } \gamma' = P\gamma \text{ for some doubly substochastic matrix } P, \tag{18}$$

i.e., by some non-negative matrix $P = (p_{ij})$ for which there exists a doubly stochastic matrix $D = (d_{ij})$ satisfying $p_{ij} \leqslant d_{ij}$ for all i, j. Similarly,

$$\gamma' \prec^{w} \gamma \text{ on } \mathbb{R}^n_+ \text{ if and only if } \gamma' = P\gamma \text{ for some doubly superstochastic matrix } P, \tag{19}$$

i.e., by some non-negative matrix $P = (p_{ij})$ for which there exists a doubly stochastic matrix $D = (d_{ij})$ satisfying $p_{ij} \geqslant d_{ij}$ for all i, j" [9].

That is, all row and column sums of a doubly substochastic matrix are at most one (equation (21)) and all row and column sums of a doubly superstochastic matrix are at least one. Now we suppose that P is doubly substochastic, and $\gamma' = P\gamma$. Then

$$\sum_{j=1}^{k} \gamma'_j = \sum_{i=1}^{n} \sum_{j=1}^{k} p_{ij}\gamma_i, \tag{20}$$

where

$$0 \leqslant \sum_{j=1}^{k} p_{ij} \leqslant 1. \tag{21}$$

In analogous manner equations (20) and (21) holds for doubly superstochastich matrices.

Since we consider a decreasing number of elements (bubbles), we like to engage in doubly substochastic matrices. In equation (22) and (23), an example for a doubly substochastic matrix is given. If each entry in a doubly stochastic matrix is diminished (while maintaining non-negativity), then a doubly substochastic matrix is obtained which maps the vector (3 1 0 0) on (2 1 0 0). The matrix diminishing the doubly stochastic matrix has negative components, it charaterizes the sink term S in equation (13).

$$\frac{1}{24}\begin{pmatrix} 17 & 7 & 0 & 0 \\ 7 & 17 & 0 & 0 \\ 0 & 0 & 17 & 7 \\ 0 & 0 & 7 & 17 \end{pmatrix} + \frac{1}{24}\begin{pmatrix} -1 & -7 & 0 & 0 \\ -1 & -11 & 0 & 0 \\ 0 & 0 & -11 & -1 \\ 0 & 0 & -7 & -1 \end{pmatrix} = \frac{1}{24}\begin{pmatrix} 16 & 0 & 0 & 0 \\ 6 & 6 & 0 & 0 \\ 0 & 0 & 6 & 6 \\ 0 & 0 & 0 & 16 \end{pmatrix}, \tag{22}$$

$$\frac{1}{24}\begin{pmatrix} 16 & 0 & 0 & 0 \\ 6 & 6 & 0 & 0 \\ 0 & 0 & 6 & 6 \\ 0 & 0 & 0 & 16 \end{pmatrix}\begin{pmatrix} 3 \\ 1 \\ 0 \\ 0 \end{pmatrix} = \begin{pmatrix} 2 \\ 1 \\ 0 \\ 0 \end{pmatrix}. \tag{23}$$

If we like to allow transitions between each diagram of the pp-structure we have to allow matrices with mixed entries too. These transitions characterize reversibility that means negative diffusion or in other words the order of the system increases (see figure 10 and diagram b_7 and a_2 for instance). It may be the Apollonian structure formation [1] in the rearrangement phase, which leads

to partially increasing order of the bubble size distributions. Other transitions are between incomparable diagrams. Incomparableness is given if the partition vectors do not satisfy equation (8). There are transitions between incomparable diagrams which follow a positive or a negative diffusion process (see the two vectors γ and γ' of figure 17 for instance) or they are only permuted (see figure 10 and diagram b_7 and b_3 for instance). In the latter case, the permutations cause the incomparableness, this may implicate a kind of weight for each row or we may say the transitions describe a kind of mixture, which consists of diffusion and drift. The reason for incomparable bubble size distributions is the same as above. The structure formation causes incomparable distributions as we have seen in this section. It is clear that if we like to take into account the total number of bubbles during the temporal development of the decay process we obtain a decreasing number of bubbles and this process is comparable to a diffusion process with a sink term. Furthermore we have seen that one possible description for diffusion processes with a sink term is the *weak majorization*. The transitions of this process consist of two matrices: a doubly stochastic matrix and a "diminishing" matrix which exclusively contains negative semidefinite entries. We can summerize that reversibility and negative diffusion, respectively, incomparableness, and diffusion with a sink term requires negative probabilities, which appear as negative components of the transition matrices. These reasons for negative probabilities we can find in our foam system and that allows us to define transition matrices with mixed components.

6. Conclusion

The representative characteristics of the foam decay are the incomparable distributions, the multi-modal distributions in the end of the rearrangement phase, and the oscillating Shannon entropy, which let us assume that the distributions partially follow a negative diffusion process. To characterize this open system with structure formation and its temporal development of the bubble size distributions we marginally change the classical majorization and the Ruch lattices. We omitted the order of the vector components with regard to the classical majorization and permitted permutations of the partition diagrams, which Ruch did not take into account in his lattices. The comparison via the partial sum vectors of the partition vectors showed a new structure (pp-structure) with exceptional properties which are comparable to the characteristics of the foam decay: the multi-modal distributions are represented by the permutations of the partition diagrams, the Shannon entropy of vicinal partition diagrams of the pp-structure behaves more or less oscillating and parts of the pp-structure describe a positive diffusion process, a negative diffusion process, and a "mixed" diffusion process. Thus the pp-structure characterizes a diffusion process without constraints.

Acknowledgments

We are indebted to G. Niehues and T. Prenzel for the *Warsteiner*-measurements.

References

[1] S. Sauerbrei, E.C. Haß, P.J. Plath, The Apollonian Decay of Beer Foam – Bubble Size Distribution and the Lattices of Young Diagrams and their Correlated Mixing Functions, submitted and accepted by Discrete Dynamics in Nature and Society.
[2] C.E. Shannon, A mathematical theory of communication, Bell Syst. Tech. J. 27 (1948) 379–423; 623–656.
[3] S. Sauerbrei, U. Sydow, P.J. Plath, On the Characterization of Foam Decay with Diagram Lattices and Majorization, submitted to Zeitschrift für Naturforschung A.
[4] E. Ruch, The diagram lattice as structural principle, Theoret. Chim. Acta (Berl.) 38 (1975) 167–183.
[5] R.F. Muirhead, Some methods applicable to identities and inequalities of symmetric algebraic functions of *n* letters, Proc. Edinb. Math. Soc. 21 (1903) 144–157.
[6] G.H. Hardy, J.E. Littlewood and G. Pólya, *Inequalities* (Cambridge University Press, London, 1934).
[7] E. Ruch and A. Schönhofer, Theorie der Chiralitätsfunktionen, Theoret. Chim. Acta (Berl.) 19 (1970) 225–287.
[8] E. Ruch, Algebraic aspects of the chirality phenomenon in chemistry, Acc. Chem. Res. 5 (1972) 49–56.
[9] A.W. Marshall and I. Olkin, *Inequalities: Theory of Majorization and Its Applications* (Academic Press, New Yark, 1979).